2.1. Introduction

Amines play an important role in life sciences and chemical industry such as pharmaceuticals, organic dyes, agrochemicals, polymers, lubricants, and more.[1],[2] Further, the amine component plays a pivotal role in the composition of drug molecules.[3],[4],[5] Due to the high importance numerous methods have been developed for the selective formation of the amines.[6],[7],[8]

The synthesis of secondary amines involves both oxidative and reductive methodologies.[9],[10],[11] In the reductive approach, carbonyl compounds react with primary amines in the presence of a suitable catalyst and stoichiometric quantities of reducing agents (e.g., borohydride, formic acid, ammonium, formate, silanes).[12],[13],[14],[15],[16] This process generates a significant amount of hazardous waste-which are difficult to handle.[12],[17],[18],[19]

Recently, tremendous progress has been achieved in oxidative C−N bond formation aiming to improve the activity and selectivity.[20],[21],[22],[23] An effective oxidative catalytic approach involves the *N*-alkylation of amines.[24],[25],[26] This method relies on borrowing hydrogen from alcohol for the hydrogenation of imine, produced through the reaction of alcohol and primary amine.[27],[28] Because of the commercial availability of the alcohols and the formation of water as the only by-product, this method has been largely followed.[29],[30],[31]

On the other hand, transition metal-based supported nanocatalysts have shown considerable potential in catalytic *N*−alkylation reactions.[32],[33],[34],[35] In this respect, the use of M−N−C@NC catalyst could be effective for the *N*−alkylation of amines following the hydrogen borrowing methodology.[36],[37],[38],[39] As mentioned in the previous chapter,[40],[41],[42] the M−N−C coordination improves the stability of the catalyst,[43],[44],[45],[46] modulates the electronic structure,[47],[48],[30],[49] and offers required selectivity for the organic

transformation reaction,[50] herein, we have demonstrated the use of Co−N−C@NC catalyst for the oxidative *N*-alkylation of amines.

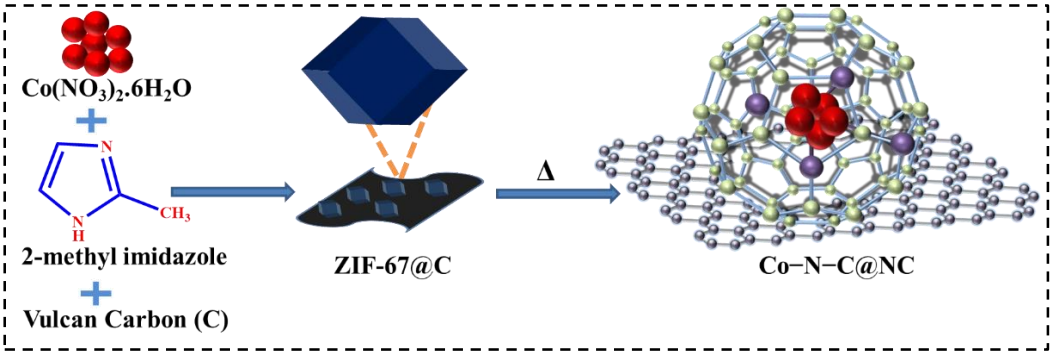

Scheme 2.1. The schematic representation for the synthesis of ZIF-67@C and its pyrolysis to produce Co−N−C@NC.

For this purpose, we have chosen ZIF-67@C as the precursor and pyrolyzed it to form Co−N−C@NC. The ZIF-67 provides a unique coordination environment around the Co-center which is maintained in Co−N−C@NC whereas the pyrolysis of the ligand produces N−doped graphene (**Scheme 2.1.**). The Co−N−C@NC works as a hydrogen-borrowing catalyst for the alkylation of the primary amines. The N−doped carbon-supported Co−N−C@NC showed excellent catalytic activity for *N*-alkylation reactions of amines and alcohols with the yield of >99 % for the desired product. Moreover, the catalyst was found to be stable enough for the recycling for six catalytic cycles without having any significant drop in the catalytic activity and selectivity.

2.2. Chemicals

Cobalt(II) nitrate hexahydrate ($Co(NO_3)_2 \cdot 6H_2O$), methanol, toluene, and silica gel were purchased from Merck Pvt. Ltd. India. 2-methylimidazole was procured from Avra, while Chloroform-D was obtained from Sigma Aldrich Pvt. Ltd. India. Vulcan-XC-72R carbon was acquired from CABOT Corporation. Substituted alcohols and amines were purchased from

Sigma Aldrich, Avra, Alfa Aesar, and SRL Pvt. Ltd. India. All catalytic experiments were carried out in a pressure sealed tube (Ace pressure tube, volume 15 mL, from Sigma).

2.3. Instruments

High-resolution X-ray diffractions (HR-XRD) of the catalysts were carried out in Rigaku SmartLab 9kW Powder X-ray diffractometer (RIGAKU Corporation). The IR spectra were measured with the Nicolet iS5 FTIR spectrometer in attenuated total reflection (ATR) mode.

Scanning Electron Microscopy (FE-SEM) studies were carried out in Nova Nano SEM 450, FEI Company of USA (S.E.A.) PTE, LTD and EVO-Scanning Electron Microscope MA15/18, Carl Zeiss Microscopy LTD, Oxford Instruments Nanoanalysis with 51 N1000-EDX System. Energy dispersive X-ray spectroscopy (EDX) images were collected by Team Pegasus Integrated EDS-EBSD with Octane plus and Hikari Pro EDX System. Elemental mapping was performed with the analyzer attached to SEM. TEM studies were carried out on Tecnai G2 20 TWIN transmission electron microscope connected with an energy-dispersive X-ray spectrometer (EDAX, r-TEM SUTW). ICP-AES was measured on a Thermo Jarrell Ash Trace Scan analyzer. The surface area was measured on a Quantachrome Autosorb-1 apparatus.

The X-ray photoelectron spectroscopy (XPS) measurements were performed in a K_α X-ray photoelectron spectrometer from Thermo Fisher Scientific and Kratos Axis Ultra X-ray photoelectron spectrometer (Kratos Analytical Ltd., Manchester, UK) with an Al Kα monochromatic radiation source (1486.7 eV). The binding energies were calibrated using the C 1s peak located at 284.6 eV as the reference. Raman spectra were recorded in an STR-300 spectrometer (AIRIX Corp.) with a 532 nm excitation source.

^{1}H NMR spectra were recorded on AVH D 500 AVANCE III HD 500 MHZ, One Bay

NMR Spectrometer from Bruker Bio Spin International. The Chemical shifts were reported in ppm. Coupling constants are expressed in Hertz (Hz). The following abbreviations are used: s = singlet, bs = broad singlet d = doublet, t = triplet and m = multiple. The residual solvent signals were used as references for ^{1}H and ^{13}C NMR spectra ($CDCl_3$: δ_H = 7.28-7.29 ppm, δ_C = 77.01-77.16 ppm). The GC-MS analyses were recorded on Agilent 5977B instrument. Conversion and yields were determined by GC-FID, HP-5MS UI chromatograph with FID detector, (HP-5MS UI .025µ, 30 m x 0.25 mm) capillary column.

2.4. Experimental

2.4.1. Synthesis of ZIF-67@C[51]

200 mg Vulcan carbon was dispersed in the 30 mL methanol and stirred for 30 minutes. 1 mmol of $Co(NO_3)_3.6H_2O$ was added in the previous solution of Vulcan carbon and stirred for 10 minutes to get dispersion solution A. (4 mmol) 2-methylimidazole was dissolved in 20 mL methanol and stirred for 10 minutes to get solution B. Further, solution B was added in solution A at a time and stirred for 24 h. The precipitate of ZIF-67@C was obtained and the precipitate was collected by centrifugation (14000 rpm) and washed five times with methanol. And the precipitate was dried at 60 ^{o}C overnight and denoted the ZIF-67@C.

2.4.2. Synthesis of Co−N−C@NC[52]

200 mg of ZIF-67@C was ground in a mortar pestle to get a fine powder. The resulting fine powder was transferred into a crucible boat and heated at 800 °C in the presence of a nitrogen atmosphere for 3 h in the tubular furnace (with heating rate: 5 °C/min starting from 35 °C). The furnace was cooled down to room temperature. Then, black powder was obtained and denoted as Co−N−C@NC.

2.4.3. Synthesis of Co@C[53]

200 mg Vulcan carbon was dispersed in 30 mL methanol and stirred for 30 minutes. 1 mmol of $Co(NO_3)_2.6H_2O$ was added in the previous solution of Vulcan carbon and stirred for 10 minutes to get dispersion solution A. 2 mmol of $NaBH_4$ was dissolved in 20 mL methanol and stirred for 10 minutes to form solution B. Further, solution B was added in solution A at a time and stirred for 24 h. The black suspension mixture of Co@C was obtained. The precipitate was obtained and the precipitate was collected by centrifugation (11000 rpm) and washed five times with methanol. The obtained precipitate was dried at 60 °C in a hot air oven overnight.

2.5. Results and discussion

2.5.1. Characterizations of the catalysts

The catalyst precursor ZIF-67@C was synthesized by the reaction of cobalt(II)nitrate and 2-methyl imidazole in the presence of Vulcan-XC-72R carbon as the support (**Scheme 2.1**). The Powder X-ray diffraction pattern (PXRD) of ZIF-67@C showed the characteristics of crystal planes (JCPDS: 08-60-513, **Figure. 2.1a**).

The pyrolysis of ZIF-67@C in the inert atmosphere at different temperatures produced Co−N−C@NC (temperature =700, 800, and 900 ^oC). The PXRD pattern of Co−N−C@NC nanoparticles showed the face-center cubic (*fcc*) crystal of cobalt (JCPDS: No.15-0806) (**Figure. 2.1b**). In Co−N−C@NC, the (111) peak of cubic cobalt was shifted towards the right side ($2\Theta = 0.3^o$) due to the coordination with nitrogen (JCPDS: 08-60-513).[54]

Further, the degree of graphitization of N−doped carbon (NC) in Co−N−C@NC was investigated by Raman spectroscopy. The Raman spectrum showed the characteristic D and G bands of carbon at 1322 cm^{-1} and 1596 cm^{-1}, respectively (Figure. 2.1(c)). The I_D/I_G ratio of 1.59 indicates the defect rich graphene structure. The classical E_g and A_{1g} vibronic modes of metallic Co were detected at 475 cm^{-1} and 682 cm^{-1}, respectively.[55],[56]

The nature of carbon was further analysed by X-ray photoelectron spectroscopy (XPS, **Figure. 2.1**). The C 1s XPS was fitted into five peaks for: sp^2 hybridised carbon of C=C (284.7 eV), sp^3 hybridised carbon C−C bond (284.9 eV), C=N (285.9 eV), C−N (287.6 eV), and COOH (290.1 eV) (**Figure 2.1d**).[57] The ratio of the graphitic carbon to other carbon is determined to be 1.62, which closely matches with the Raman data.

The N 1s XPS was deconvulated into four peaks at binding energies 398.1, 399.0, 400.8, and 401.7 eV corresponding to pyridinic, Co−N, pyrrolic, and graphitic nitrogen (**Figure 2.1e**). This result confirms the doping of N in the carbon matrix and the formation of the Co−N bond.[58] Therefore, in the Co−N−C@NC, the Co atoms are coordinated to the pyrolic−N and

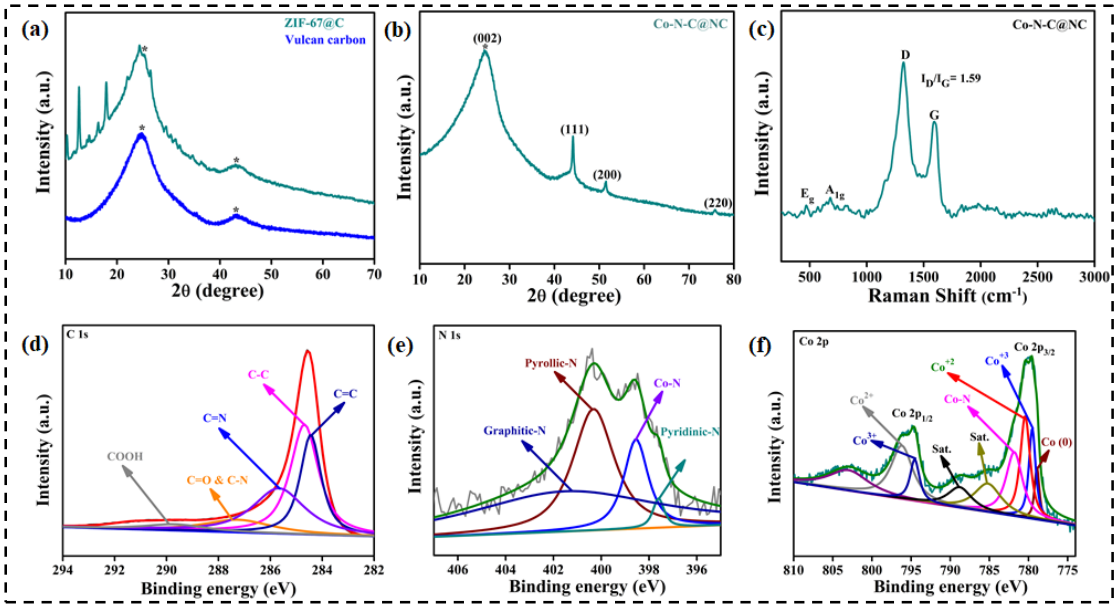

Figure 2.1. (a) The PXRD graph of ZIF-67@C and Vulcan carbon. (b) & (c) shows the PXRD and Raman spectra of the graph of the Co−N−C@NC. (d) The C 1s spectrum of Co−N−C@NC was deconvoluted into five peaks for C=C, C−C, C=N, C−N, and COOH species. (e) The N 1s spectrum was fitted into four peaks- corresponding to pyridinic, Co−N, pyrrolic, and graphitic nitrogen. (f) Co 2p XPS was fitted into peaks for Co(0), Co−N, Co(III), and Co(II) species. The * marked peaks are originated as the satellite peaks of Co(II). (d) O 1s spectrum of Co−N−C@NC.

pyridinic−N and offer active sites during catalytic reaction.

The Co 2p XPS was fitted into two peaks-corresponding to Co $2p_{3/2}$ (780.1 eV) and Co $2p_{1/2}$ (795.3 eV) (**Figure 2.1f**). The Co $2p_{3/2}$ peak was further deconvoluted into the peaks for Co^0 (779.3 eV) and Co−N (782.3 eV), Co(III) (779.9 eV), and Co(II) (780.8 eV) species. The presence of Co(III) and Co(II) species can be explained by the surface oxidation of cobalt nanoparticles.[59]

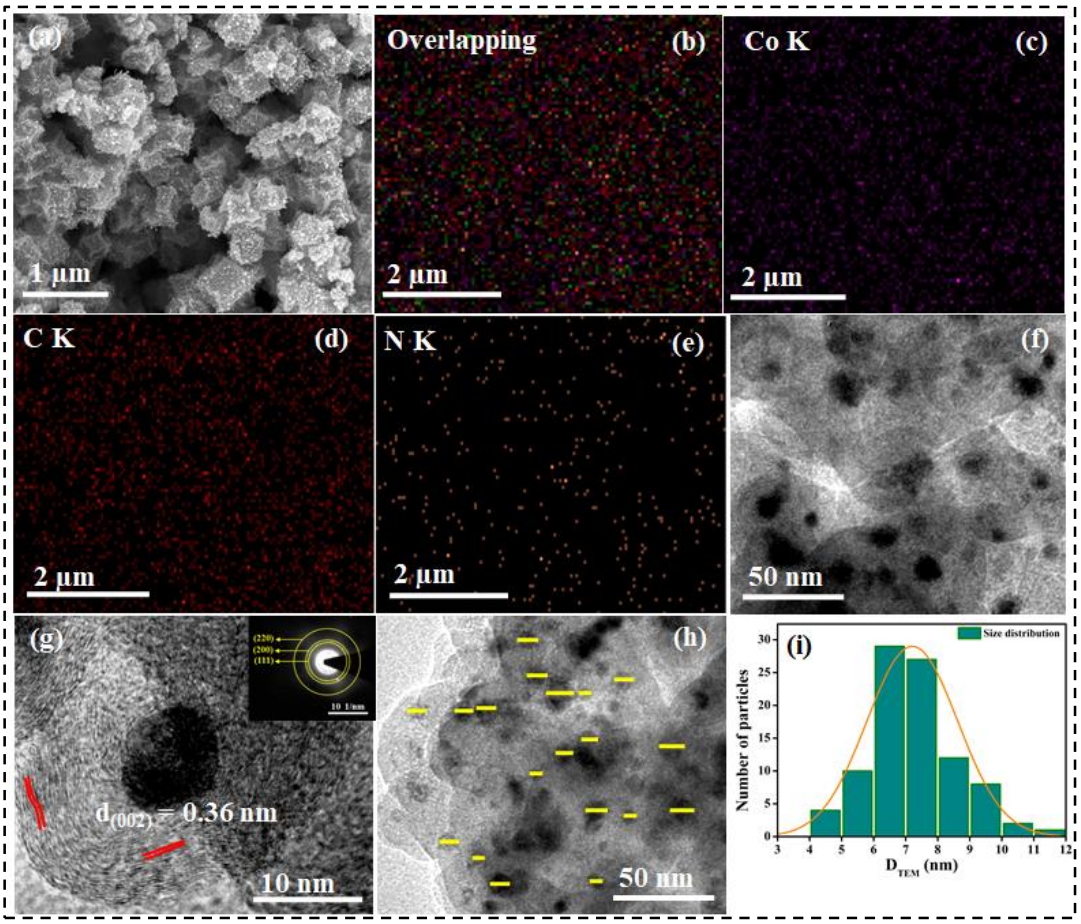

Figure 2.2. (a) FE-SEM image of Co−N−C@NC showing the rhombic dodecahedron morphology of the particles. (b-e) elemental mapping of Co−N−C@NC, (f) TEM images of Co−N−C@NC with spherical morphology. (g) HR-TEM image showing the inter-planar spacing between the graphene layers and inset SAED pattern of the Co−N−C@NC. (h-i) The size of the particles was calculated to be 4-12 nm.

The scanning electron microscopy (SEM) images showed rhombic dodecahedron morphology of Co−N−C@NC where the Co nanoparticles were densely embedded on NC (**Figure 2.2a**). The energy-dispersive X-ray (EDX) spectrum of Co−N−C@NC revealed the presence of Co, N, and C whereas the EDX elemental mapping showed the homogeneous distribution of Co on N−doped carbon (**Figure 2.2b-e**).

Further, the morphological detail of the catalyst was confirmed by transmission electron microscopy (TEM, **Figure 2.2f**). The selected area electron diffraction (SAED) pattern of Co−N−C@NC showed the diffraction rings corresponding to the crystal planes (111), (200), and (220) of *fcc* cobalt (**Figure 2.2g-inset**). The inter-planar spacing of the N−doped carbon layer was calculated to be 0.36 nm, corresponding to the (002) plane of graphene (**Figure 2.2g**). The TEM images of Co−N−C@NC demonstrated that the Co nanoparticles with varying sizes (4-12 nm) were distributed in the N−doped carbon frameworks (**Figure 2.2h-i**).

2.6. Optimization of the catalytic reaction conditions

First, the catalytic performance of Co−N−C@NC was optimized for the *N*-alkylation reaction of benzyl alcohol and aniline (**Table 2.1**). The reaction of benzyl alcohol with aniline can produce *N*-benzylaniline (**2a**) and *N*-benzyleneaniline (**2a′**) as the major products. Therefore, control over the selectivity to produce **2a** as the major product is a challenging task. The hydrogen borrowing route can be effectively employed to synthesize *N*-benzylaniline.

Interestingly, Co−N−C@NC was found to be highly selective for the production of **2a** when full conversion was achieved. For the comparison purpose, we used Co@C and found that the coordination of Co with N is extremely important for improved selectivity and activity. While Co−N−C@NC can produce **2a** with 99% yield after the full conversion (**Entry 1, Table2.1**), Co@C can reach the maximum yield of 65% (87% conversion) under the same reaction

conditions (**Entry 4, Table 2.1**). The other catalysts had poor conversion and low selectivity for **2a** (**Entries 5-7, Table 2.1**).

Table 2.1. Optimization of the reaction condition

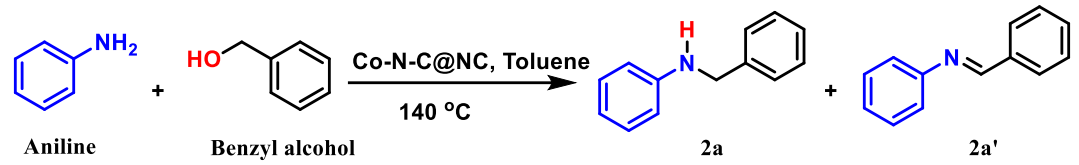

Entry	Catalyst	Base	Solvent	Conv. (%)	Yield **2a** (%)	Yield **2a'** (%)
Variation of catalyst						
1.	**Co-N-C@NC**	***tert*-BuOK**	**Toluene**	**>99**	**99**	0
2.	Co-N-C@NC -1	*tert*-BuOK	Toluene	96	87	9
3.	Co-N-C@NC -2	*tert*-BuOK	Toluene	>99	90	9
4.	Co@C	*tert*-BuOK	Toluene	87	65	22
5.	Vulcan carbon	*tert*-BuOK	Toluene	35	28	7
6.	Co-ZIF@C	*tert*-BuOK	Toluene	56	46	9
7.	$Co(NO_3)_2.6H_2O$	*tert*-BuOK	Toluene	44	36	8
Variation of base						
8.	Co-N-C@NC	-	Toluene	85	56	29
9.	Co-N-C@NC	K_2CO_3	Toluene	54	40	14
10.	Co-N-C@NC	Cs_2CO_3	Toluene	65	56	9
11.	Co-N-C@NC	KOH	Toluene	86	73	13
12.	**Co-N-C@NC**	***tert*-BuOK**	**Toluene**	**>99**	**99**	0
13.	Co-N-C@NC	*tert*-BuOK(0.1 mmol)	Toluene	88	76	12
14.	Co-N-C@NC	*tert*-BuOK(0.3 mmol)	Toluene	94	88	6
15.	Co-N-C@NC	*tert*-BuOK(0.5 mmol)	Toluene	>99	99	0
Variation of catalyst amount						
16.	Co-N-C@NC (5 mg)	*tert*-BuOK	Toluene	85	76	8
17.	**Co-N-C@NC (10 mg)**	***tert*-BuOK**	**Toluene**	**>99**	**99**	0
18.	Co-N-C@NC (15 mg)	*tert*-BuOK	Toluene	>99	92	6
Variation of solvent						
19.	Co-N-C@NC	*tert*-BuOK	CH_3CN	54	43	9
20.	Co-N-C@NC	*tert*-BuOK	Dioxane	91	80	11
21.	Co-N-C@NC	*tert*-BuOK	THF	97	86	11
22.	**Co-N-C@NC**	***tert*-BuOK**	**Toluene**	**>99**	**99**	0

Reaction conditions: Benzyl alcohol (1 mmol), aniline (0.5 mmol), catalyst (10 mg), toluene (2 mL), *tert*-BuOK (0.5 mmol), temperature (140 ^oC) and time 18 h. We have also optimized with different reaction temperature (120, 130 and 140 ^oC to obtained 85, 96 and 99% yields). Conversion and selectivity were detected by GC-MS and ^1H-NMR.

The pyrolysis temperature of the catalysts has also a significant effect on the conversion and selectivity of the products. Comparison of the catalysts prepared at different pyrolysis temperatures (700-900 ^{o}C), it was found that Co−N−C@NC (prepared at 800 ^{o}C) produced the best activity and selectivity for **2a** (**Entries 1-3, Table 2.1**).

Further, the effect of different bases on the yield of **2a** has been determined. The yield of **2a** dropped in the absence of base and in the presence of bases, the yield of **2a** followed the order: *tert*-BuOK > KOH > Cs_2CO_3 > K_2CO_3 (**Entries 8-12, Table 2.1**). And the different amount of base also affect the yield of **2a** product (**Entries 13-15, Table 2.1**).The optimized amount of the Co−N−C@NC catalyst was found to be 10 mg and a poorer yield of **2a** was obtained with lower (5 mg) or higher (15 mg) amount of catalyst (**Entries 16-18, Table 2.1**). Next, we optimized the effect of solvent, and the best conversion and selectivity for **2a** was recorded in toluene. Other non-polar aprotic solvents also produced high selectivity with the following order: toluene > THF > dioxane > acetonitrile (**Entries 19-22, Table 2.1**). In polar protic solvents like methanol and ethanol, we observed the formation of a mixture of products and we did not continue the reaction further.

2.7. Scope of different alcohols

With the optimized reaction conditions, the *N*-alkylation of aniline with different benzyl alcohols was studied (Scheme 2.2, **2a-2k,** and Table 2.2). In all the cases, secondary amines (**2**) were found to be the major product (yield = 81-99 %). The best yield (99 %) was obtained for the reaction of aniline with benzyl alcohol after 18 h of reaction (**Scheme 2.2, 2a and table 2.2**). The methoxy-substitution at the *para*-position of benzyl alcohol slowed down the reaction but the yield of the secondary amine **2b** was not affected. However, a decrease in the yield of **2c** was observed when 2,4-dimthoxy-benzyl alcohol was reacted with aniline, most probably

due to the increasing steric hindrance. On the other hand, the electron-withdrawing substituent

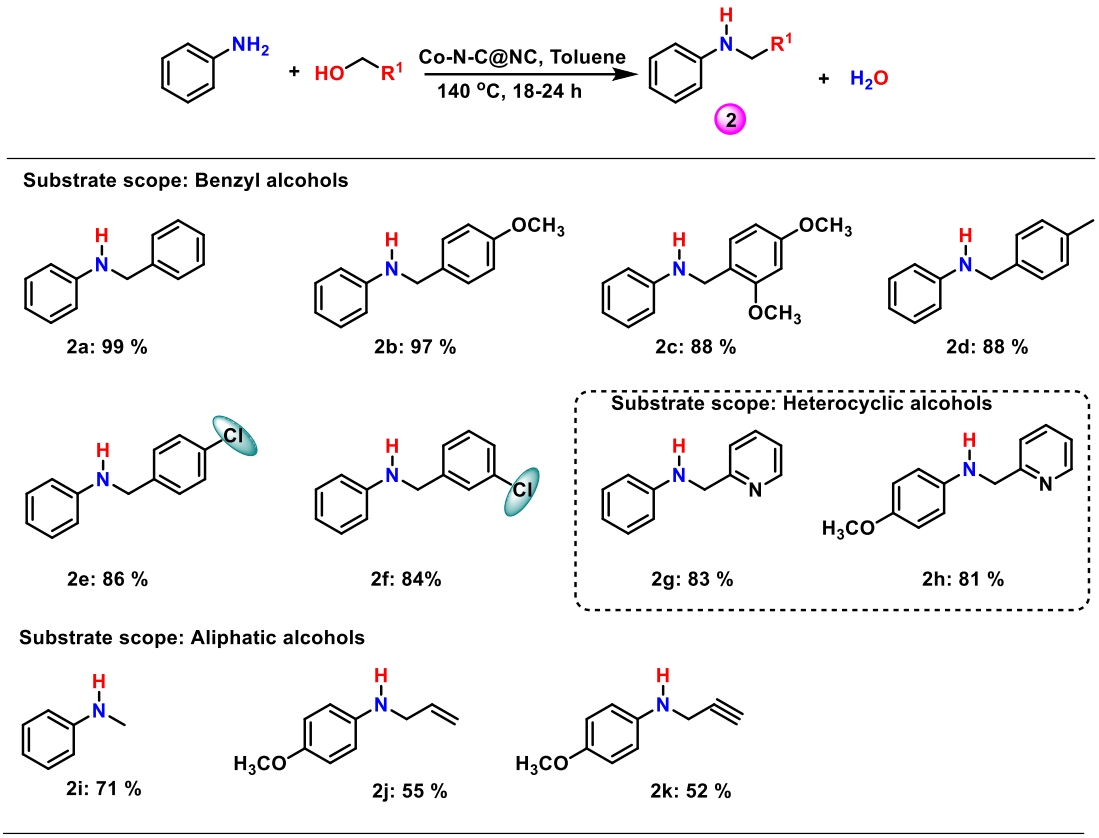

Scheme 2.2. *N*-alkylation of aniline and substituted-anilines with different benzyl alcohols using Co−N−C@NC catalyst. Reaction conditions: 1 mmol substituted benzyl alcohol, 0.5 mmol aniline, 10 mg catalyst, 0.5 mmol *tert*-BuOK, 2 mL toluene, 140 °C, 24 h. For 3a (18 h), 3e (18 h) and 3f (18 h) optimized at different time.

in the *meta*- and *para*- position of benzyl alcohol slightly decreases the yield of the corresponding secondary amines when reacted with aniline (**Scheme 2.2, 2d-2f and table 2.2**). The use of heterocyclic benzyl alcohol (pyridine-2-yl-methanol) decreased the yield of **2g** and **2h** (**Scheme 2.2, Table 2.2**). The aliphatic alcohols were found to produce lower yield (52-71%) for *N*-alkylation than the benzylic alcohols (**Scheme 2.2, 2j-2l and Table 2.2**). The yield of N-alkylated product decreased from methanol to propylene alcohol to propyne alcohol.

2.8. Scope of different anilines

Next, we explored the scope of different anilines for *N*-alkylation reactions with benzyl alcohol. Anilines with different electron donating and electron withdrawing substituents in the factor on the product yield was not clear (**Scheme 2.3 and Table 2.2**). However, a series of phenyl ring produced high yield (>80%) for secondary amines and the effect of the electronic substituted anilines were selectively converted into secondary amines. The effect of steric

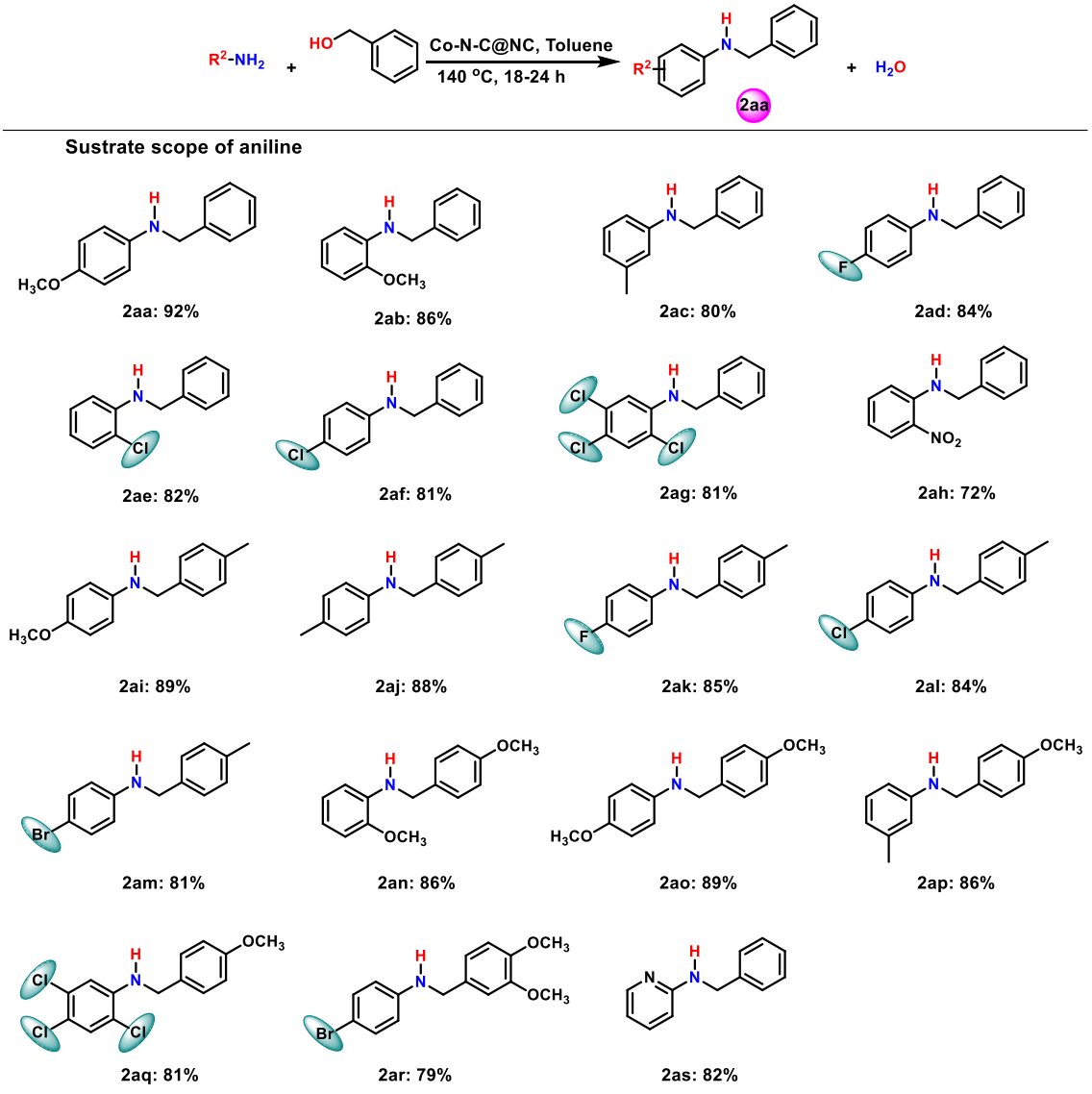

Scheme 2.3. Co−N−C@NC catalyzed the *N*-alkylation reaction of different anilines with benzyl alcohols. Reaction condition:1 mmol substituted benzyl alcohol, 0.5 mmol aniline, 10 mg catalyst, 0.5 mmol *tert*-BuOK, 2 mL toluene, 140 °C, 24 h. For 4d (18 h), 4e (20 h), and 4f (20 h) optimized at different times.

crowding is distinct and the substitution in the *ortho*-position of anilines resulted in low yields (**Scheme 2.3, 2ab, 2ae, 2ag, 2ah, 2an, 2aq**). The lowest yield (72%) among the studied substituted anilines was obtained with 2-nitroanililine due to the introduction of both steric crowding and electron-withdrawing effect (**Scheme 2.3, 2ah**).

When the steric crowding in both substrates was increased, a significant drop in the yield of the product was observed (**Scheme 2.3, 2aq-2ar**). Even, heterocyclic aniline with benzyl alcohol produced high yield of secondary heterocyclic amines (**Scheme 2.2, 2as**). Therefore, Co−N−C@NC is highly efficient in catalysing the *N*-alkylation of a series of anilines with different alcohols (benzyl alcohols, aliphatic primary alcohols, allylic alcohol, and alkyne alcohol).

2.9. Reaction path and mechanism

To get an insight of the reaction pathway, the advancement of the reaction with time was monitored. The reaction of benzyl alcohol with aniline produced both *N*-benzylene aniline (imine) and *N*-benzylaniline (secondary amine) (**Figure 2.3a**). The time-dependent profile of the products clearly indicates that a consecutive reaction mechanism is followed for the formation of *N*-benzylaniline. Initially, the yield of the imine was high and converted to *N*-benzylaniline with time (**Figure 2.3a**). The hydrogen borrowing reaction mechanism was also established by a series of controlled reactions (**Figure 2.3a**). According to hydrogen borrowing methodology, the first step is the dehydrogenation of benzyl alcohol by [Co] to form as the major product when aniline was not introduced in the reaction mixture (**Figure 2.3c**). Separately, the reaction of 4-methoxy benzaldehyde and 4-methoxy aniline in the presence of Co−N−C@NC produced imine as the major product by the condensation process (**Figure 2.3c**). The absence of hydrogen borrowing process in the first step hindered the formation of

H−[Co]− H and hence the production of secondary amine by the hydrogenation of imine was restricted (**Figure 2.3c**). These reactions have clearly established that the first step is the dehydrogenation of benzyl alcohol to form benzaldehyde, which undergoes condensation with aniline to form imine, followed by the hydrogenation of imine to form secondary amine. The catalyst Co−N−C@NC provides active sites for all the three processes-dehydrogenation, condensation, and hydrogenation.

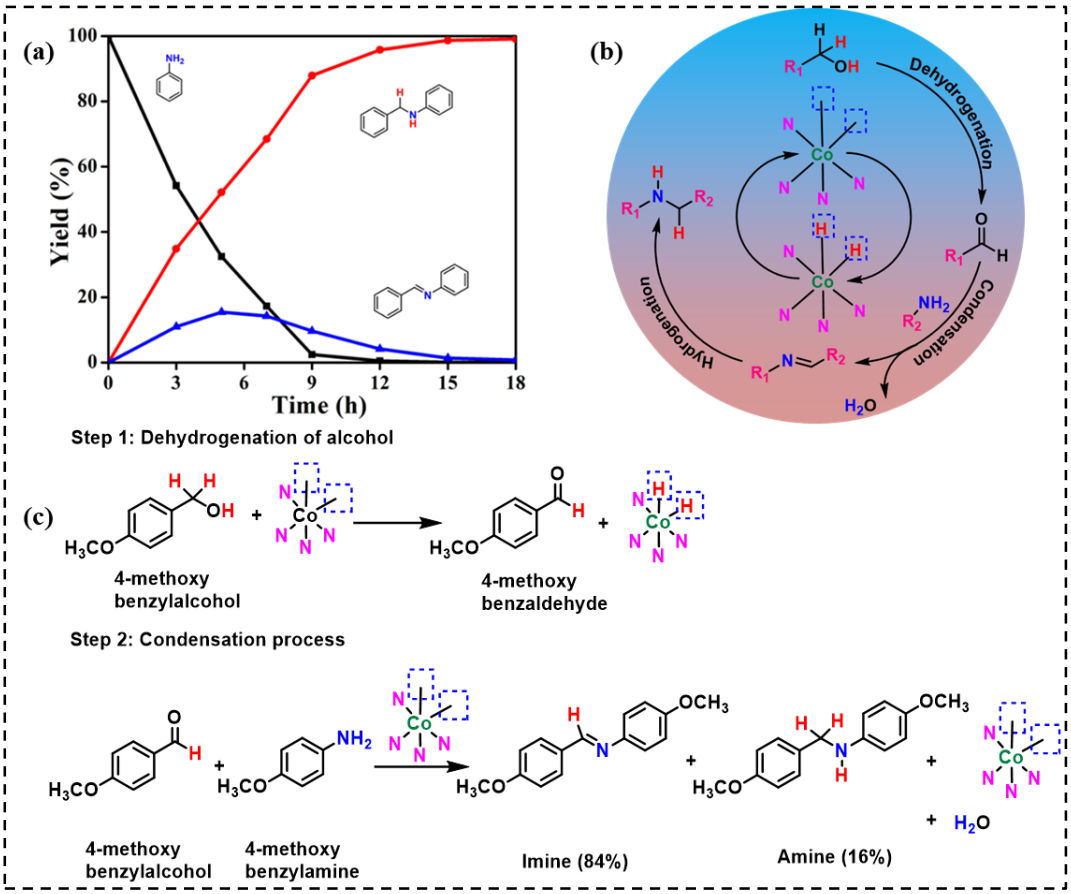

Figure 2.3. (a) Progress of the *N*-alkylation reaction of aniline and benzyl alcohol with time**. (b)** Reaction mechanism for the *N*-alkylation reactions**. (c)** Sequence of the reaction involved as detected by ^{1}H NMR.

2.10. Recycling of the catalyst

We have investigated the recyclability of Co−N−C@NC for the *N*-alkylation reaction of aniline and benzyl alcohol. After each reaction, the catalyst was separated from the reaction

mixture by centrifugation and used for a new batch of reaction. The catalyst was recycled six times with a minor loss in the activity and yield (**Figure 2.4**). After, the recyclability of the catalyst, the catalyst was leached out 0.50% during the reaction.

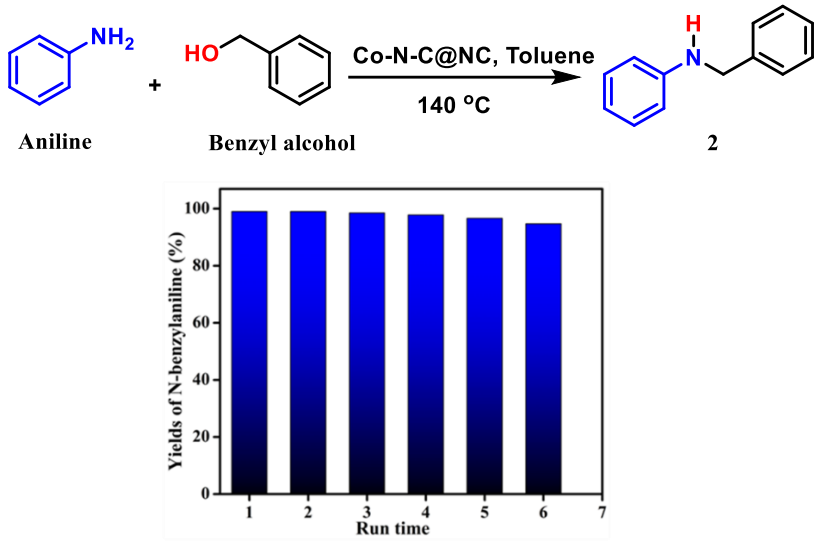

Figure 2.4. Recycling test of Co−N−C@NC for the synthesis of *N*-benzylaniline. Reaction conditions: 1 mmol benzyl alcohol, 0.5 mmol aniline, 10 mg catalyst, 0.5 mmol *tert*-BuOK, 2 mL toluene, 140 °C, 24 h. Conversions and yields are based on aniline and determined by GC.

2.11. Conclusions

In conclusion, ZIF-67-derived Co−N−C@NC catalysts have been developed for the *N*-alkylation of anilines with alcohols to produce secondary amines. In Co−N−C@NC, the Co−N coordination, accessed through the pyrolysis of MOF, was found to be beneficial to modulate the electron density on cobalt, optimize the binding of the substrates and reaction intermediates on the catalyst surface, and improve the yield of the desired product. The scope of a series of alcohols and anilines were explored and moderate to high yield of secondary amine was observed depending on the substrates. Moreover, the catalyst has remarkable stability and versatile substrate scope for the synthesis of secondary amines.

Table 2.2. Characterization of the products by ^{1}H NMR and ^{13}C NMR

Note: For some compounds intensity of -NH peak is poor and hence not properly visible in ^{1}HNMR.

2a: *N*-benzylaniline 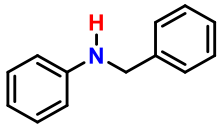 **2a**	**^{1}H NMR (500 MHz, $CDCl_3$):** δ 7.43-7.31 (m, *J* = 7.1 Hz, 5H), 7.23 (m, *J* = 7.4 Hz, 2H), 6.77 (m, *J* = 7.3 Hz, 1H), 6.69 (d, *J* = 8.5 Hz, 2H), 4.38 (s, 2H), 4.07 (s, 1H). **^{13}C NMR (126 MHz, $CDCl_3$):** δ 148.12, 139.40, 129.24, 128.6, 127.48, 127.20, 117.53, 112.81, 48.28. Yield of product: 99%, 90.2 mg and 0.49 mmol, liquid, blood red.
2b: *N*-(4methoxybenzyl) aniline 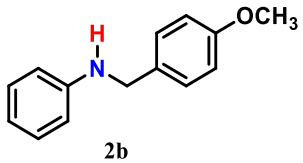 **2b**	**^{1}H NMR (500 MHz, $CDCl_3$)** δ 7.33 (d, *J* = 8.6 Hz, 2H), 7.21 (d, *J* = 8.5, 7.4 Hz, 2H), 6.92 (d, *J* = 8.7 Hz, 2H), 6.75 (m, *J* = 7.3 Hz, 1H), 6.67 (d, *J* = 7.6 Hz, 2H), 4.29 (s, 2H), 3.98 (s, 1H), 3.84 (s, 3H). **^{13}C NMR (126 MHz, $CDCl_3$)** δ 158.89, 148.24, 131.44, 129.28, 128.84, 117.53, 114.05, 112.86, 55.33, 47.82. Yield of product: 97%, 103.6 mg, 0.48 mmol and solid dark red.
2c: *N*-(2,4-dimethoxybenzyl) aniline 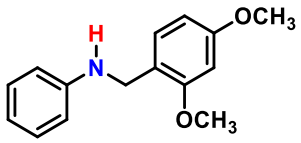 **2c**	**^{1}H NMR (500 MHz, $CDCl_3$)** δ 7.26–7.20 (m, 2H), 7.19 (d, *J* = 1.2 Hz, 2H), 6.71 (t, *J* = 6.8 Hz, 1H), 6.68 (d, *J* = 7.6 Hz, 2H), 6.50 (d, *J* = 2.3 Hz, 1H), 6.46 (m, *J* = 8.3, 2.4 Hz, 2H), 4.28 (s, 2H), 3.86 (s, 3H), 3.82 (s, 3H), 3.41 (s, 1H). **^{13}C NMR (126 MHz, $CDCl_3$)** δ 160.22, 158.45, 148.52, 129.71, 129.16, 119.80, 117.30, 113.12, 103.92, 98.65, 55.39, 43.18. Yield of product: 88%, 107.1 mg, 0.44 mmol and solid red.
2d: *N*-(4-methylbenzyl) aniline 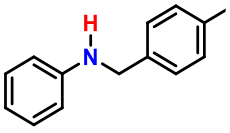 **2d**	**^{1}H NMR (500 MHz, $CDCl_3$)** δ 7.34 (t, *J* = 7.7 Hz, 2H), 7.25 (dd, *J* = 13.3, 5.9 Hz, 4H), 6.79 (m, *J* = 10.2 Hz, 1H), 6.71 (d, *J* = 7.3 Hz, 2H), 4.36 (s, 2H), 4.04 (s, 1H), 2.44 (s, 3H). **^{13}C NMR (126 MHz, $CDCl_3$)** δ 148.31, 136.92, 136.46, 129.35, 127.59, 117.56, 112.92, 48.14, 21.18. Yield of product: 88%, 86.8 mg and 0.44 mmol, solid, orange.
2e: *N*-(4-chlorobenzyl) aniline 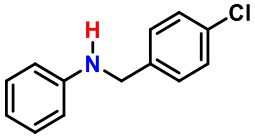 **2e**	**^{1}H NMR (500 MHz, $CDCl_3$)** δ 7.33 (d, 4H), 7.25–7.18 (m, 2H), 6.76 (t, *J* = 7.3 Hz, 1H), 6.64 (d, *J* = 8.4 Hz, 2H), 4.34 (s, 2H), 4.09 (s, 1H). **^{13}C NMR (126 MHz, $CDCl_3$)** δ 147.94, 138.12, 132.98, 129.42, 128.84, 117.92, 113.00, 47.72. Yield of product: 86%, 94.0 mg, 0.43 mmol and liquid light yellow.
2f: *N*-(3-chlorobenzyl)aniline 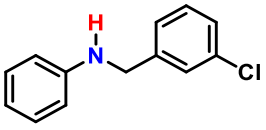 **2f**	**^{1}H NMR (500 MHz, $CDCl_3$)** δ 7.40 (s, 1H), 7.28 (t, 3H), 7.24–7.18 (m, 2H), 6.77 (m, *J* = 7.3 Hz, 1H), 6.65 (d, *J* = 7.7 Hz, 2H), 4.35 (s, 2H), 4.12 (s, 1H). **^{13}C NMR (126 MHz, $CDCl_3$)** δ 147.79, 141.75, 134.54, 129.89, 129.31, 127.40, 125.41, 117.87, 112.91, 47.80. Yield of product: 84%, 91.8 mg, 0.42 mmol and liquid green.

2g: *N*-(pyridine-2-ylmethyl) aniline 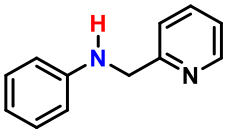 **2g**	**^{1}H NMR (500 MHz, $CDCl_3$)** δ 8.60 (m, 1H), 7.66 (td, *J* = 1.8, 7.7 Hz, 1H), 7.36 (dt, *J* = 1.0, 7.8 Hz, 1H), 7.23–7.17 (m, 3H), 6.74 (m,1H), 6.69 (t, *J* = 7.7 Hz, 2H), 5.12–4.62 (m, 1H), 4.49 (s, 2H). **^{13}C NMR (126 MHz, $CDCl_3$)** δ 158.91, 149.58, 148.26, 137.06, 129.63, 122.50, 121.99, 117.99, 113.44, 49.67. Yield of product: 83%, 76.4 mg, 0.415 mmol and liquid dark red.
2h: 4-methoxy-*N*-(pyridin-2-ylmethyl) aniline 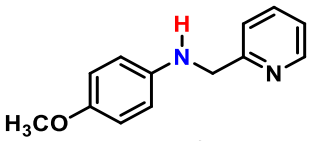 **2h**	**^{1}H NMR (500 MHz, $CDCl_3$)** δ 8.60 (d, *J* = 5.6 Hz, 1H), 7.65 (t, *J* = 7.7 Hz, 1H), 7.36 (d, *J* = 7.6 Hz, 1H), 7.22–7.16 (m, 1H), 6.80 (d, *J* = 8.9 Hz, 2H), 6.65 (d, *J* = 8.0 Hz, 2H), 4.44 (s, 2H), 3.86 (s, 1H), 3.76 (s, 3H). **^{13}C NMR (126 MHz, $CDCl_3$)** δ 158.89, 152.26, 149.21, 142.19, 136.64, 122.07, 121.68, 114.92, 114.33, 55.79, 50.28. Yield of product: 81%, 86.5 mg, 0.40 mmol and solid wine color.
2i: *N*-benzylpyridin-2-amine 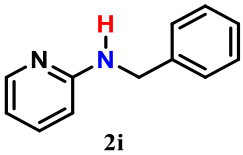 **2i**	**^{1}H NMR (500 MHz, $CDCl_3$)** δ 8.11 (d, *J* = 4.2 Hz, 1H), 7.49–7.31 (m, 5H), 7.32–7.26 (m, 1H), 6.67–6.56 (m, 1H), 6.39 (d, *J* = 8.4 Hz, 1H), 5.11 (s, 1H), 4.53 (d, *J* = 4.7 Hz, 2H). **^{13}C NMR (126 MHz, $CDCl_3$)** δ 158.74, 148.17, 139.24, 137.68, 128.75, 127.41, 113.23, 106.89, 46.42. Yield of product: 82%, 75.5 mg, 0.41 mmol and liquid dark red.
2j: *N*-methylaniline 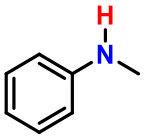 **2j**	**^{1}H NMR (500 MHz, $CDCl_3$)** δ 7.27 (t, *J* = 7.9 Hz, 2H), 6.79 (t, *J* = 8.3 Hz, 1H), 6.69 (d, *J* = 7.8 Hz, 2H), 3.71 (s, 1H), 2.89 (s, 3H). **^{13}C NMR (126 MHz, $CDCl_3$)** δ 149.42, 129.26, 117.29, 112.48, 30.76. Yield of product: 72%, 39.1 mg, 0.36 mmol, and liquid wine.
2k: *N*-allylaniline 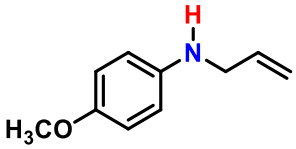 **2k**	**^{1}H NMR (500 MHz, $CDCl_3$):** δ 6.81 (d, *J* = 9.0 Hz, 2H), 6.63 (d, *J* = 8.9 Hz, 2H), 5.99 (ddd, *J* = 15.7, 10.4, 5.2 Hz, 1H), 5.31 (dd, *J* = 17.2, 1.7 Hz, 1H), 5.19 (dd, *J* = 10.3, 1.5 Hz, 1H), 3.77 (s, 3H), 3.76 (d, *J* = 5.5 Hz, 2H). **^{13}C NMR (126 MHz, $CDCl_3$):** δ 152.25 (s), 142.32 (s), 135.84 (s), 116.14 (s), 114.90 (s), 114.36 (s), 55.82 (s), 47.58 (s). Yield of product: 55%, 41.6 mg, 0.27 mmol, and liquid blood red.
2l: 4-methoxy-*N*-(prop-2-yn-1-yl) aniline 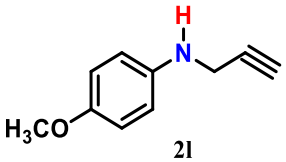 **2l**	**^{1}H NMR (500 MHz, $CDCl_3$):** ^{1}H NMR (500 MHz, $CDCl_3$) δ 6.85 (d, *J* = 9.0 Hz, 2H), 6.70 (d, *J* = 9.0 Hz, 2H), 3.91 (s, 2H), 3.78 (s, 3H), 2.24 (s, 1H). **^{13}C NMR (126 MHz, $CDCl_3$):** δ 153.01, 140.97, 115.14, 114.86, 81.43, 71.26, 55.73, 34.60. Yield of product: 52%, 42.4 mg, 0.26 mmol, and liquid blood red.
2aa: *N*-benzyl-4-methoxyaniline 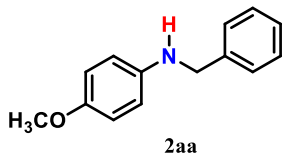 **2aa**	**^{1}H NMR (500 MHz, $CDCl_3$):** δ 7.48-7.39 (m, 4H), 7.35 (t, *J* = 6.7 Hz, 1H), 6.86 (d, *J* = 8.8 Hz, 2H), 6.68 (d, *J* = 8.7 Hz, 2H), 4.35 (s, 2H), 3.81 (s, 3H), 3.63 (s, 1H). **^{13}C NMR (126 MHz, $CDCl_3$)** δ 152.25, 142.55, 139.81, 128.68, 127.63, 127.24, 114.99, 114.19, 55.85, 49.28. Yield of product: 92%, 98.1 mg, 0.46 mmol, and solid dark red.

2ab: *N*-benzyl-2-methoxyaniline 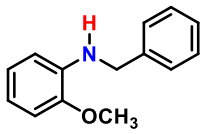 **2ab**	**^{1}H NMR (500 MHz, $CDCl_3$)** δ 7.38 (m, *J* = 7.3 Hz, 5H), 6.89 (t, *J* = 7.6 Hz, 1H), 6.84 (d, *J* = 7.8 Hz, 1H), 6.73 (t, *J* = 7.5 Hz, 1H), 6.65 (d, *J* = 7.8 Hz, 1H), 4.69 (s, 1H), 4.40 (s, 2H), 3.90 (s, 3H). **^{13}C NMR (126 MHz, $CDCl_3$)** δ 146.90, 139.69, 138.23, 128.69, 127.63, 127.23, 121.39, 116.76, 110.21, 109.50, 55.52, 48.16. Yield of product: 86%, 91.7 mg, 0.40 mmol, and solid white crystal.
2ac: *N*-benzyl-3-methylaniline 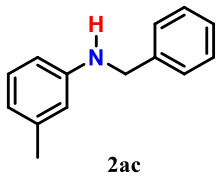 **2ac**	**^{1}H NMR (500 MHz, $CDCl_3$)** δ 7.40-7.25 (m, 5H), 7.15-7.06 (m, 1H), 6.63 (t, *J* =0.8, 1H), 6.57-6.50 (m, 2H), 4.38 (s, 2H), 4.02 (s, 1H), 2.35 (s, 3H). **^{13}C NMR (126 MHz, $CDCl_3$)** δ 148.31, 139.65, 139.13, 129.25, 128.72, 127.63, 127.29, 118.62, 113.73, 110.05, 48.42, 21.75. Yield of product: 80%, 78.9 mg, 0.40 mmol, and solid white crystal.
2ad: *N*-benzyl-4-fluoroaniline 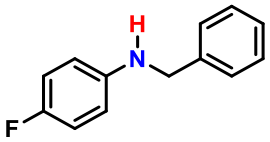 **2ad**	**^{1}H NMR (500 MHz, $CDCl_3$)** δ 7.38-7.30 (m, 4H), 7.30-7.25 (m, 1H), 6.95-6.92 (d, *J* = 7.7 Hz, 2H), 6.62-6.57 (d, *J* = 13.1 Hz, 2H), 4.33 (s, 2H), 3.97 (s, 1H). **^{13}C NMR (126 MHz, $CDCl_3$)** δ 156.68, 154.81, 144.35, 139.10, 128.53, 127.35, 115.44, 113.53, 48.78. Yield of product: 84%, 84.5 mg, 0.40 mmol, and liquid greenish.
2ae: *N*-benzyl-2-chloroaniline 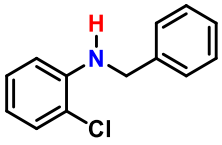 **2ae**	**^{1}H NMR (500 MHz, $CDCl_3$)** δ 7.45–7.39 (m, 3H), 7.39–7.29 (m, 5H), 6.73 – 6.71 (d, 1H), 4.77 (s, 1H), 4.39 (s, 2H). **^{13}C NMR (126 MHz, $CDCl_3$)** δ 143.38, 137.66, 131.78, 129.94, 129.02, 127.87, 127.42, 119.50, 117.83, 112.31, 47.95. Yield of product:81%, 88.16 mg, 0.405 mmol and liquid light yellow
2af: *N*-benzyl-4-chloroaniline 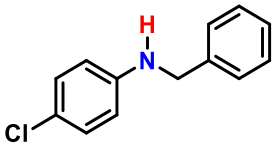 **2af**	**^{1}H NMR (500 MHz, $CDCl_3$)** δ 7.38 (d, *J* = 4.6 Hz, 4H), 7.32 (dd, *J* = 8.7, 4.5 Hz, 1H), 7.14 (d, *J* = 8.9 Hz, 2H), 6.57 (d, *J* = 8.9 Hz, 2H), 4.32 (s, 2H), 4.07 (s, 1H). **^{13}C NMR (126 MHz, $CDCl_3$)** δ 146.70, 139.13, 129.12, 128.76, 127.45, 122.12, 113.98, 48.37. Yield of product: 82%, 88.2 mg, 0.405 mmol and liquid greenish.
2ag: *N*-benzyl-2,4,5-trichloroaniline 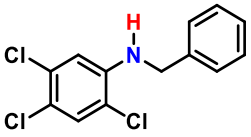 **2ag**	^{1}H NMR (500 MHz, $CDCl_3$) δ 7.42-7.33 (m, 6H), 6.71 (s, 1H), 4.76 (s, 1H), 4.38 (s, 2H). ^{13}C NMR (126 MHz, $CDCl_3$) δ 137.68, 131.80, 129.96, 129.04, 127.88, 127.43, 119.53, 117.86, 112.33, 47.97. Yield of product: 81%, 116.23 mg, 0.40 mmol, and solid greenish.
2ah: *N*-benzyl-2-nitroaniline 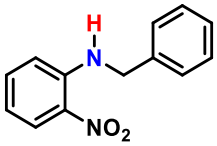 **2ah**	**^{1}H NMR (600 MHz, $CDCl_3$)** δ 8.46 (s, 1H), 8.22 (d, *J* = 8.6 Hz, 1H), 7.43 – 7.31 (m, 6H), 6.84 (d, 1H), 6.69 (, 1H), 4.57 (s, 2H). **^{13}C NMR (151 MHz, $CDCl_3$)** δ 145.27, 137.37, 136.24, 132.29, 128.95, 127.72, 127.06, 126.89, 115.74, 114.21, 47.11. Yield of product: 72%, 82.2 mg, 0.36 mmol and solid yellow.

2ai: 4-methoxy-*N*-(4-methylbenzyl) aniline 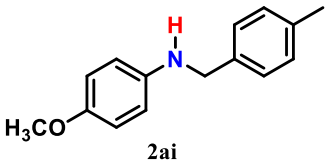 **2ai**	**^{1}H NMR (500 MHz, $CDCl_3$)** δ 7.29 (d, *J* = 9.0 Hz, 2H), 7.18 (d, *J* = 7.9 Hz, 2H), 6.81 (d, *J* = 8.9 Hz, 2H), 6.64 (d, *J* = 8.9 Hz, 2H), 4.27 (s, 2H), 3.78 (s, 3H), 2.38 (s, 3H). **^{13}C NMR (126 MHz, $CDCl_3$)** δ 152.26, 142.65, 136.93, 136.71, 129.39, 127.68, 115.02, 114.24, 55.94, 49.13, 21.23. Yield of product: 89%, 101.4 mg, 0.44 mmol and solid red.
2aj: 4-methyl-*N*-(4-methylbenzyl) aniline 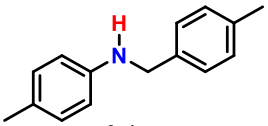 **2aj**	**^{1}H NMR (500 MHz, $CDCl_3$)** δ 7.33 (d, *J* = 7.7 Hz, 2H), 7.22 (d, *J* = 7.6 Hz, 2H), 7.05 (d, *J* = 7.9 Hz, 2H), 6.63 (d, *J* = 8.1 Hz, 2H), 4.32 (s, 2H), 3.91 (s, 1H), 2.41 (s, 3H), 2.31 (s, 3H). **^{13}C NMR (126 MHz, $CDCl_3$)** δ 146.07, 136.81, 136.66, 129.79, 129.33, 127.56, 126.71, 113.06, 48.46, 21.15, 20.45. Yield of product: 88%, 73.23 mg, 0.44 mmol, and solid white crystal.
2al: 4-chloro-*N*-(4-methylbenzyl) aniline 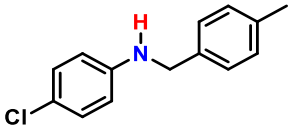 **2al**	**^{1}H NMR (500 MHz, $CDCl_3$)** δ 7.29-7.26 (m, 2H), 7.20 (d, *J* = 7.4 Hz, 2H), 7.15 (d, *J* = 8.8 Hz, 2H), 6.58 (d, *J* = 8.8 Hz, 2H), 4.29 (s, 2H), 4.05 (s, 1H), 2.39 (s, 3H). **^{13}C NMR (126 MHz, $CDCl_3$)** δ 146.74, 137.05, 135.89, 129.39, 129.07, 127.44, 122.03, 113.92, 48.13, 21.13. Yield of product: 84%, 97.5 mg, 0.42 mmol, and solid white.
2am: 4-bromo-*N*-(4-methylbenzyl) aniline 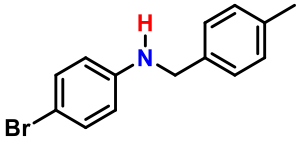 **2am**	**^{1}H NMR (500 MHz, $CDCl_3$)** δ 7.31-7.25 (m, 4H), 7.20 (d, *J* = 7.8 Hz, 2H), 6.53 (d, *J* = 8.8 Hz, 2H), 4.29 (s, 2H), 4.07 (s, 1H), 2.39 (s, 3H). **^{13}C NMR (126 MHz, $CDCl_3$)** δ 147.16, 137.08, 135.83, 131.94, 129.41, 127.44, 114.44, 109.05, 48.02, 21.13 Yield of product: 81%, 112.1 mg, 0.406 mmol, and solid white.
2an: *N*-(4-methoxybenzyl)-2-methoxyaniline 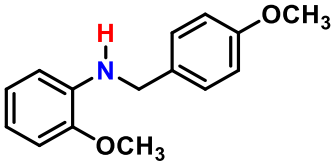 **2an**	**^{1}H NMR (500 MHz, $CDCl_3$)** δ 7.33 (d, *J* = 8.6 Hz, 2H), 6.91 (d, *J* = 8.7 Hz, 2H), 6.87 (t, *J* = 7.6 Hz, 1H), 6.81 (d, *J* = 9.2 Hz, 1H), 6.70 (t, *J* = 8.5 Hz, 1H), 6.64 (d, *J* = 9.2 Hz, 1H), 4.63 (s, 1H), 4.30 (s, 2H), 3.86 (s, 3H), 3.83 (s, 3H). **^{13}C NMR (126 MHz, $CDCl_3$)** δ 158.92, 146.91, 138.30, 131.68, 128.96, 121.40, 116.72, 114.14, 110.20, 109.49, 55.48, 47.66. Yield of product: 86%, 104.8 mg, 0.43 mmol and solid wine red.
2ao: *N*-(4-methoxybenzyl)-4-methoxyaniline 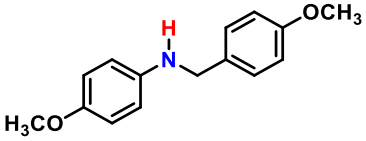 **2ao**	**^{1}H NMR (500 MHz, $CDCl_3$)** δ 7.30 (d, *J* = 8.6 Hz, 2H), 6.89 (d, *J* = 6.8 Hz, 2H), 6.79 (d, *J* = 8.9 Hz, 2H), 6.62 (d, *J* = 8.9 Hz, 2H), 4.22 (s, 2H), 3.81 (s, 3H), 3.75 (s, 3H). **^{13}C NMR (126 MHz, $CDCl_3$)** δ 158.84, 152.19, 142.55, 131.70, 128.86, 114.93, 114.08, 55.84, 55.32, 48.76. Yield of product: 89%, 108.3 mg, 0.44 mmol, and solid green.
2ap: *N*-(4-methoxybenzyl)-3-methylaniline 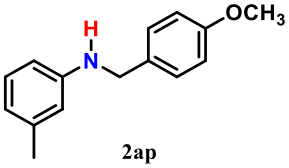 **2ap**	**^{1}H NMR (500 MHz, $CDCl_3$)** δ 7.31 (d, *J* = 8.7 Hz, 2H), 7.09 (t, *J* = 7.7 Hz, 1H), 6.91 (d, *J* = 8.7 Hz, 2H), 6.57 (d, *J* = 7.4 Hz, 1H), 6.51-6.46 (m, 2H), 4.26 (s, 2H), 3.97 (s, 1H), 3.83 (s, 3H), 2.30 (s, 3H). **^{13}C NMR (126 MHz, $CDCl_3$)** δ 158.96, 148.36, 139.17, 131.63, 129.27, 128.98, 118.64, 114.14, 113.78, 110.13, 55.44, 47.99, 21.77. Yield of product: 86%, 98.12 mg, 0.43 mmol, and solid light yellow.

2aq: 2,4,5-trichloro-*N*-(4-methoxybenzyl) aniline 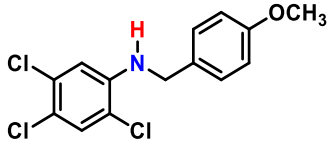 **2aq**	**^{1}H NMR (500 MHz, $CDCl_3$)** δ 7.36 (s, 1H), 7.29 (d, *J* = 5.3 Hz, 2H), 6.93 (d, *J* = 8.7 Hz, 2H), 6.72 (s, 1H), 4.66 (s, 1H), 4.30 (s, 2H), 3.84 (s, 3H). **^{13}C NMR (126 MHz, $CDCl_3$)** δ 159.21, 143.32, 131.66, 129.82, 129.50, 128.70, 119.29, 117.71, 114.29, 112.21, 55.34, 47.39. Yield of product: 81%, 128.7 mg, 0.40 mmol and solid light green.
2ar: 4-bromo-*N*-(3,4-dimethoxybenzyl) aniline 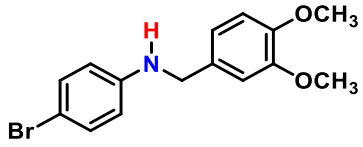 **2ar**	**^{1}H NMR (500 MHz, $CDCl_3$)** δ 7.31-7.22 (d, 2H), 6.91 (d, *J* = 8.3 Hz, 2H), 6.87 (s, 1H), 6.53 (d, *J* = 8.7 Hz, 2H), 4.24 (s, 2H), 4.05 (s, 1H), 3.89 (s, 6H). **^{13}C NMR (126 MHz, $CDCl_3$)** δ 149.25, 148.39, 147.16, 131.94, 131.39, 119.65, 116.71, 114.47, 111.32, 110.74, 77.06, 55.91, 48.18. Yield of product: 79%, 127.6 mg, 0.39 mmol, and solid green crystal.

2.12. ^{1}H NMR and ^{13}C NMR spectra of product

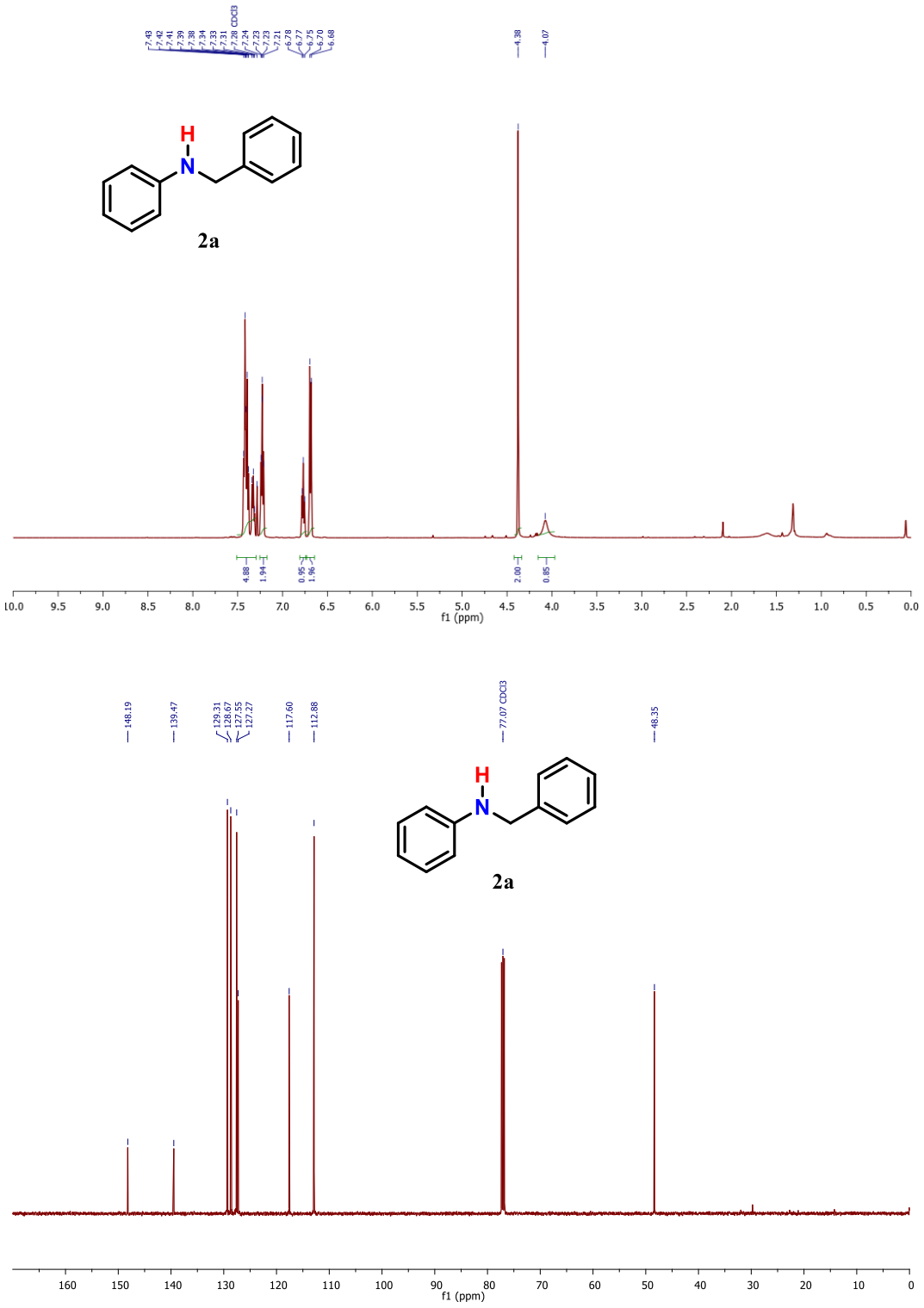

Figure 2.5: ^{1}H NMR and ^{13}C NMR spectra of the compound **2a**.

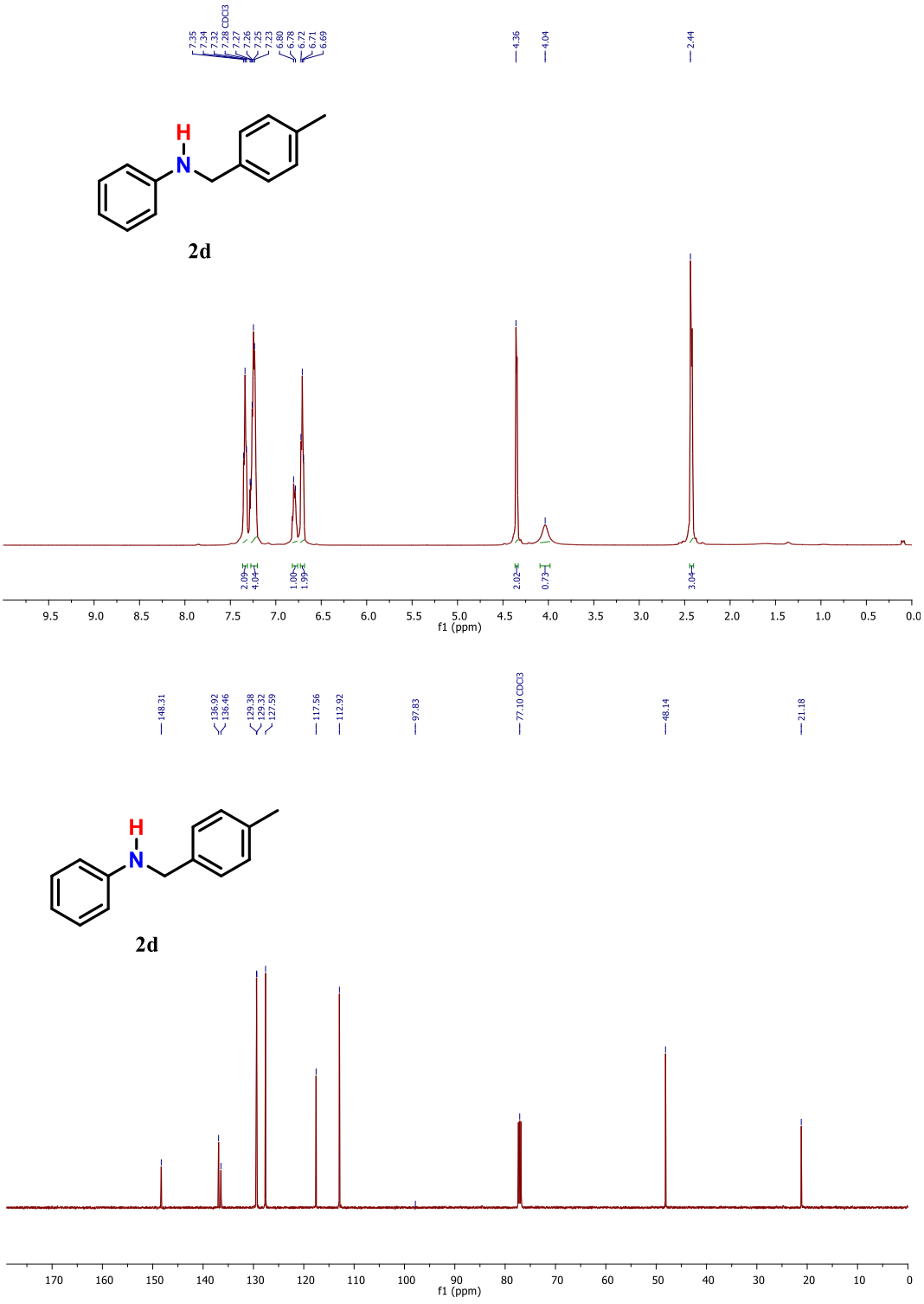

Figure 2.6: ^{1}H NMR and ^{13}C NMR spectra of the compound **2d**.

2.13. References

[1] S. Elangovan, J. Neumann, J. B. Sortais, K. Junge, C. Darcel, M. Beller, *Nat. Commun.* **2016**, *7*, 1–8.

[2] Y. Wang, F. L. Zhang, Z. J. Liu, Z. J. Yao, *Inorg. Chem.* **2022**, *61*, 10310–10320.

[3] S. Chakraborty, R. Mondal, S. Pal, A. K. Guin, L. Roy, N. D. Paul, *J. Org. Chem.* **2023**, *88*, 771–787.

[4] A. Corma, J. Navas, M. J. Sabater, *Chem. Rev.* **2018**, *118*, 1410–1459.

[5] A. S. Santos, A. M. S. Silva, M. M. B. Marques, *European J. Org. Chem.* **2020**, *2020*, 2501–2516.

[6] J. Bariwal, E. Van Der Eycken, *Chem. Soc. Rev.* **2013**, *42*, 9283–9303.

[7] C. Chaudhari, S. M. A. H. Siddiki, K. Kon, A. Tomita, Y. Tai, K. I. Shimizu, *Catal. Sci. Technol.* **2014**, *4*, 1064–1069.

[8] K. Chakrabarti, M. Maji, S. Kundu, *Green Chem.* **2019**, *21*, 1999–2004.

[9] J. I. Ramsden, R. S. Heath, S. R. Derrington, S. L. Montgomery, J. Mangas-Sanchez, K. R. Mulholland, N. J. Turner, *J. Am. Chem. Soc.* **2019**, *141*, 1201–1206.

[10] C. Zhang, Q. Liang, W. Yang, G. Zhang, M. Hu, G. Zhang, *Green Chem.* **2022**, *24*, 7368–7375.

[11] S. Rojas-Buzo, P. Concepción, A. Corma, M. Moliner, M. Boronat, *ACS Catal.* **2021**, *11*, 8049–8061.

[12] K. Murugesan, T. Senthamarai, V. G. Chandrashekhar, K. Natte, P. C. J. Kamer, M. Beller, R. V. Jagadeesh, *Chem. Soc. Rev.* **2020**, *49*, 6273–6328.

[13] R. Cano, D. J. Ramón, M. Yus, *J. Org. Chem.* **2011**, *76*, 5547–5557.

[14] L. Wang, X. Jv, R. Wang, L. Ma, J. Liu, J. Sun, T. Shi, L. Zhao, X. Zhang, B. Wang, *ACS Sustain. Chem. Eng.* **2022**, *10*, 8342–8349.

[15] V. Goyal, J. Gahtori, A. Narani, P. Gupta, A. Bordoloi, K. Natte, *J. Org. Chem.* **2019**, *84*, 15389–15398.

[16] P. Tomkins, C. Valgaeren, K. Adriaensen, T. Cuypers, D. E. D. Vos, *ChemCatChem* **2018**, *10*, 3689–3693.

[17] E. Pedrajas, I. Sorribes, K. Junge, M. Beller, R. Llusar, *Green Chem.* **2017**, *19*, 3764–3768.

[18] E. Podyacheva, O. I. Afanasyev, D. V Vasilyev, D. Chusov, **2022**, DOI 10.1021/acscatal.2c01133.

[19] N. Deibl, R. Kempe, *Angew. Chemie - Int. Ed.* **2017**, *56*, 1663–1666.

[20] M. H. S. A. Hamid, C. L. Allen, G. W. Lamb, A. C. Maxwell, H. C. Maytum, A. J. A. Watson, J. M. J. Williams, *J. Am. Chem. Soc.* **2009**, *131*, 1766–1774.

[21] J. J. A. Celaje, X. Zhang, F. Zhang, L. Kam, J. R. Herron, T. J. Williams, *ACS Catal.* **2017**, *7*, 1136–1142.

[22] T. T. Dang, B. Ramalingam, S. P. Shan, A. M. Seayad, *ACS Catal.* **2013**, *3*, 2536–2540.
[23] T. Ohshima, Y. Miyamoto, J. Ipposhi, Y. Nakahara, M. Utsunomiya, K. Mashima, *J. Am. Chem. Soc.* **2009**, *131*, 14317–14328.
[24] P. Ruiz-Castillo, S. L. Buchwald, *Chem. Rev.* **2016**, *116*, 12564–12649.
[25] O. Saidi, A. J. Blacker, M. M. Farah, S. P. Marsden, J. M. J. Williams, *Chem. Commun.* **2010**, *46*, 1541–1543.
[26] C. Li, K. F. Wan, F. Y. Guo, Q. H. Wu, M. L. Yuan, R. X. Li, H. Y. Fu, X. L. Zheng, H. Chen, *J. Org. Chem.* **2019**, *84*, 2158–2168.
[27] B. G. Reed-Berendt, D. E. Latham, M. B. Dambatta, L. C. Morrill, *ACS Cent. Sci.* **2021**, *7*, 570–585.
[28] M. Stratakis, H. Garcia, *Chem. Rev.* **2012**, *112*, 4469–4506.
[29] T. Irrgang, R. Kempe, *Chem. Rev.* **2019**, *119*, 2524–2549.
[30] J. Gao, R. Ma, L. Feng, Y. Liu, R. Jackstell, R. V. Jagadeesh, M. Beller, *Angew. Chem. Int. Ed.* **2021**, *60*, 18591–18598.
[31] S. Mhadmhan, M. D. Marquez-Medina, A. A. Romero, P. Reubroycharoen, R. Luque, *Molecules* **2019**, *24*, 24152695.
[32] P. Y. Wu, G. P. Lu, C. Cai, *Green Chem.* **2021**, *23*, 396–404.
[33] V. Goyal, N. Sarki, A. Narani, G. Naik, K. Natte, R. V. Jagadeesh, *Coord. Chem. Rev.* **2023**, *474*, 214827.
[34] K. I. Shimizu, K. Kon, W. Onodera, H. Yamazaki, J. N. Kondo, *ACS Catal.* **2013**, *3*, 112–117.
[35] A. Afanasenko, S. Elangovan, M. C. A. Stuart, G. Bonura, F. Frusteri, K. Barta, *Catal. Sci. Technol.* **2018**, *8*, 5498–5505.
[36] H. Liu, G. K. Chuah, S. Jaenicke, *J. Catal.* **2015**, *329*, 262–268.
[37] M. Dixit, M. Mishra, P. A. Joshi, D. O. Shah, *Catal. Commun.* **2013**, *33*, 80–83.
[38] F. Kallmeier, R. Fertig, T. Irrgang, R. Kempe, *Angew. Chem. Int. Ed.* **2020**, *59*, 11789–11793.
[39] K. Natte, H. Neumann, R. V. Jagadeesh, M. Beller, *Nat. Commun.* **2017**, *8*, 1–9.
[40] Z. An, J. Li, *Green Chem.* **2022**, *24*, 1780–1808.
[41] B. Singh, A. Indra, *Mater. Today Chem.* **2020**, *16*, 100239.
[42] S. Ma, W. Han, W. Han, F. Dong, Z. Tang, *J. Mater. Chem. A* **2023**, *11*, 3315–3363.
[43] C. Li, Y. Meng, S. Yang, H. Li, *ChemCatChem* **2021**, *13*, 5166–5177.
[44] S. Rösler, M. Ertl, T. Irrgang, R. Kempe, *Angew. Chem. Int. Ed.* **2015**, *54*, 15046–15050.
[45] A. Tomer, F. Wyrwalski, C. Przybylski, J. F. Paul, E. Monflier, M. Pera-Titus, A. Ponchel, *J. Catal.* **2017**, *356*, 111–124.

[46] H. Su, K. X. Zhang, B. Zhang, H. H. Wang, Q. Y. Yu, X. H. Li, M. Antonietti, J. S. Chen, *J. Am. Chem. Soc.* **2017**, *139*, 811–818.

[47] A. Indra, T. Song, U. Paik, *Adv. Mater.* **2018**, *30*, 1–25.

[48] Z. Ma, B. Zhou, X. Li, R. G. Kadam, M. B. Gawande, M. Petr, R. Zbořil, M. Beller, R. V. Jagadeesh, *Chem. Sci.* **2022**, *13*, 111–117.

[49] A. Bähr, G. H. Moon, H. Tüysüz, *ACS Appl. Energy Mater.* **2019**, *2*, 6672–6680.

[50] G. Li, H. Yang, H. Zhang, Z. Qi, M. Chen, W. Hu, L. Tian, R. Nie, W. Huang, *ACS Catal.* **2018**, *8*, 8396–8405.

[51] T. Y. Su, G. P. Lu, K. K. Sun, M. Zhang, C. Cai, *Catal. Sci. Technol.* **2022**, *12*, 2106–2121.

[52] Z. Zhang, Q. Yu, Y. Dai, B. Feng, *Colloids Surfaces A Physicochem. Eng. Asp.* **2023**, *657*, 130559.

[53] X. Song, S. Sun, W. Zhang, Z. Yin, *J. Colloid Interface Sci.* **2004**, *273*, 463–469.

[54] X. Liu, L. Xu, G. Xu, W. Jia, Y. Ma, Y. Zhang, *ACS Catal.* **2016**, *6*, 7611–7620.

[55] H. Pan, D. Wu, X. Huang, K. Xie, B. He, Z. Lu, P. Liu, J. Cheng, X. Zhao, J. Masa, X. Chen, *J. Electrochem. Soc.* **2019**, *166*, 479–486.

[56] Y. Xue, N. N. T. Pham, G. Nam, J. Choi, Y. Y. Ahn, H. Lee, J. Jung, S. G. Lee, J. Lee, *Chem. Eng. J.* **2021**, *408*, 127305.

[57] A. K. Singh, S. Ji, B. Singh, C. Das, H. Choi, P. W. Menezes, A. Indra, *Mater. Today Chem.* **2022**, *23*, 100668.

[58] Z. Lin, G. Waller, Y. Liu, M. Liu, C. P. Wong, *Adv. Energy Mater.* **2012**, *2*, 884–888.

[59] C. Yuan, J. Li, L. Hou, X. Zhang, L. Shen, X. W. Lou, *Adv. Funct. Mater.* **2012**, *22*, 4592–4597.